Journal of Power Sources 236 (2013) 341–349

Contents lists available at SciVerse ScienceDirect

Journal of Power Sources

journal homepage: www.elsevier.com/locate/jpowsour

Effects of temperature and pressure on the performance of a solid oxide fuel cell running on steam reformate of kerosene

Larry A. Chick*, Olga A. Marina, Chris A. Coyle, Ed C. Thomsen

Pacific Northwest National Laboratory, 904 Battelle Blvd., Richland, WA 99352, USA

HIGHLIGHTS

- Tested button SOFC at pressures up to 724 kPa and temperatures from 650 °C to 800 °C.
- Open circuit voltages increased with pressure as predicted by the Nernst equation.
- At 750 °C, 0.8 V power boost due to kinetics was ~1/2 as large as boost due to OCV.
- Impedance spectroscopy showed a decrease in electrodic losses at elevated pressures.
- Power densities increased nearly linearly with the logarithm of pressure.

ARTICLE INFO

Article history:
Received 8 August 2012
Received in revised form
13 November 2012
Accepted 30 November 2012
Available online 10 December 2012

Keywords:
Solid oxide fuel cell
Pressure effect
Temperature effect
Steam reformate of kerosene

ABSTRACT

A button solid oxide fuel cell with a $La_{0.6}Sr_{0.4}Co_{0.2}Fe_{0.8}O_3$ cathode and a nickel-YSZ anode was tested over a range of temperatures from 650 to 800 °C and a range of pressures from 101 to 724 kPa. The fuel was simulated steam-reformed kerosene and the oxidant was air. The observed increases in open circuit voltages (OCVs) at elevated pressures were accurately predicted by the Nernst equation. Kinetics also increased with the pressure, although the power boost due to improved kinetics was just more than half as large as the boost due to increased OCV. The power boost increased almost linearly with the logarithm of pressure. At constant voltage the relative power boost due to increased pressure was higher at higher temperatures. At constant current the relative power boost was the same for all temperatures. When the pressure was increased from 101 to 724 kPa, the total power boost at 750 °C and 0.8 V was 66%. A significant decrease in electrodic losses at elevated pressures was observed by impedance spectroscopy. Complex impedance spectra were dominated by a combination of low frequency processes that decreased markedly with increasing pressure. A composite of high-frequency processes also decreased with pressure, but to a lesser extent.

1. Introduction

Many researchers have proposed hybrid power systems, combining solid oxide fuel cells (SOFCs) and gas turbines, in which the SOFCs are assumed to be operated at elevated pressure [1–7]. However, there is scant experimental data in the literature on effects of pressure on SOFC performance. Singhal [8] reported data collected on doped lanthanum manganite cathode-supported tubular cells at 1000 °C in the pressure range 101–1520 kPa with 89% hydrogen fuel. The electrolyte was yttria-stabilized zirconia (YSZ) and the anode was Ni-YSZ. The power boost on a pressure increase from 101 kPa to 1013 kPa at 0.7 V was 62%. Minh [9] reported data at 800 °C at 101, 203 and 304 kPa obtained from a Ni/YSZ anode-supported cell with a thin YSZ electrolyte and lanthanum strontium manganite (LSM) cathode. The fuel composition was not reported. The power boost due to increasing the pressure from 101 kPa to 304 kPa at 0.8 V was 36%. Lim et al. [11] reported on a pressurized test of a 5 kW stack with planar, anode-supported cells. Tests were performed up to 355 kPa at 800 °C. The fuel was pre-reformed natural gas. The power boost on increasing the pressure from 101 kPa to 203 kPa at 0.8 V was 65%. Zhou et al. [12] tested an anode-supported tubular SOFC at temperatures of 650, 700, 750 and 800 °C and pressures up to 608 kPa. The fuel was moist hydrogen. The power boost due to increasing the pressure from 101 kPa to 405 kPa at 750 °C and 0.8 V was 23%. The power boost due to increasing the temperature from 700 °C to 750 °C at 101 kPa and 0.8 V was 32%. Hashimoto et al. [13,14] tested an anode-supported micro-tubular cell at 650 °C

* Corresponding author. Tel.: +1 509 375 2145; fax: +1 509 375 2186.
E-mail address: larry.chick@pnnl.gov (L.A. Chick).

0378-7753/$ – see front matter © 2013 Elsevier B.V. All rights reserved.
http://dx.doi.org/10.1016/j.jpowsour.2012.11.136

from 101 to 700 kPa in 31% H_2, balance N_2, with air on the cathode. The power boost due to increasing the pressure from 101 kPa to 700 kPa at 0.8 V was 103%. Jensen et al. [15] ran an anode-supported planar cell both in SOFC mode and as a solid oxide electrolyzer. The SOFC tests were performed at 750 °C from 40 to 1000 kPa with oxygen on the cathode and either 50% H_2 or 20% H_2, balance H_2O on the anode. The power boost due to increasing the pressure from 101 kPa to 1000 kPa at 0.8 V was 63%. Seidler et al. [16] tested a 5 cell stack composed of anode-supported cells each with an active area of 84 cm^2 at temperatures of 750 and 800 °C and pressures from 140 to 300 kPa. The 50° increase in temperature had a much larger effect on power density than the 160 kPa increase in pressure. The power boost due to increasing the pressure from 140 kPa to 300 kPa at 800 °C and 0.8 V was 7%. The power boost due to increasing the temperature from 750 °C to 800 °C at 300 kPa and 0.8 V was 37%. Henke et al. [17] reported on tests of a 5-cell flow-through stack running at pressures from 135 to 800 kPa. The temperature was 800 °C. The fuel was 30% H_2, balance N_2 and fuel utilization varied from 30 to 50%. Results showed that, for a given voltage or current density, power density increased logarithmically with pressure, as predicted previously in their theoretical study [18]. The power boost due to increasing pressure from 135 to 800 kPa at 30% fuel utilization was 68%. The Fuel Cell Handbook [10] stated that the effect of pressure follows the relation:

$$\Delta Vp(mV) = 59 \log(P_1/P_2). \quad (1)$$

This appears to be derived from the Nernst equation at ~900 °C for a four electron process and is only related to the change in the OCV.

Of course, it is straightforward to calculate the effect of pressure on OCV via the Nernst equation:

$$OCV = (RT/4F)*\ln(PO_{2\ cathode}/PO_{2\ anode}), \quad (2)$$

where R is the gas constant (J (mol·K)$^{-1}$), T is the temperature (K), F is the Faraday constant (coulomb mol^{-1}) and $PO_{2\ cathode}$ and $PO_{2\ anode}$ are the partial pressures of oxygen over the cathode and anode, respectively. Since $PO_{2\ cathode}$ is given by the mole fraction of oxygen multiplied by the total pressure, P_{total}, it changes with pressure, whereas $PO_{2\ anode}$ does not change with pressure (for a given ratio of H_2 to H_2O) because it is given by

$$PO_{2\ anode} = \left(P_{H_2O}/(P_{H_2}*K_p)\right)^2, \quad (3)$$

where P_{H_2O} and P_{H_2} are the partial pressures of steam and hydrogen and K_p is the equilibrium constant. Then,

$$PO_{2\ anode} = \left(([H_2O]*P_{total})/([H_2]*P_{total}*K_p)\right)^2, \quad (4)$$

where $[H_2O]$ and $[H_2]$ are the mole fractions of steam and hydrogen. Examination of Equation (4) shows that the P_{total} cancels out and does not affect $PO_{2\ anode}$. Therefore, assuming ideal gas behavior, because $PO_{2\ cathode}$ changes with total pressure and $PO_{2\ anode}$ does not, the OCV changes with pressure (Equation (2)).

However, it is reasonable to expect that changing total pressure should also affect the kinetics of the SOFC electrode reactions and therefore should affect the slope and/or curvature of the current–voltage (I–V) curve. Examination of the I–V curves given by Minh [9] (slide 24) and Zhou [12] (upper portions of the I–V curves in Fig. 2) do indeed show changes in both slope and curvature. These effects of pressure on kinetics are difficult to predict [18,19] and can be expected to change with different electrode materials [20].

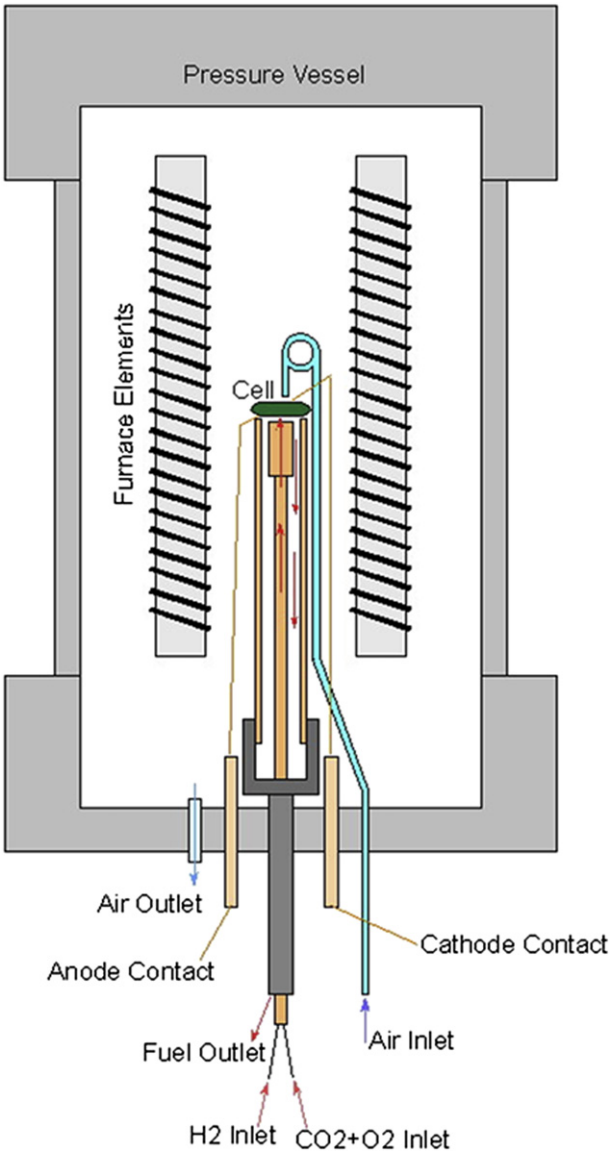

Fig. 1. Schematic of high pressure test stand.

In this paper we report on experiments conducted on a button SOFC cell over ranges of temperature and pressure. The results are discussed and compared to those in the literature.

2. Experimental

2.1. Cell fabrication

An anode supported button cell with an active area of 2 cm^2 was used. The anode was ~480 μm Ni-YSZ, the electrolyte was ~8 μm of 8 mol YSZ, the barrier layer on the cathode side was ~2–3 μm of $Sm_{0.2}Ce_{0.8}O_2$ and the cathode was ~35 μm of $La_{0.6}Sr_{0.4}Co_{0.2}Fe_{0.8}O_3$ (LSCF). The anode current collector was a disk of Ni mesh attached with NiO paste and fired to 800 °C. The cathode current collector was Ag mesh attached with Ag paste and dried before assembly. The anode side of the cell was sealed onto the alumina test fixture with barium aluminosilicate glass by heating to 850 °C while air flowed to both sides of the cell. The anode was then reduced using H_2 at 800 °C. A schematic of the test stand is shown in Fig. 1.

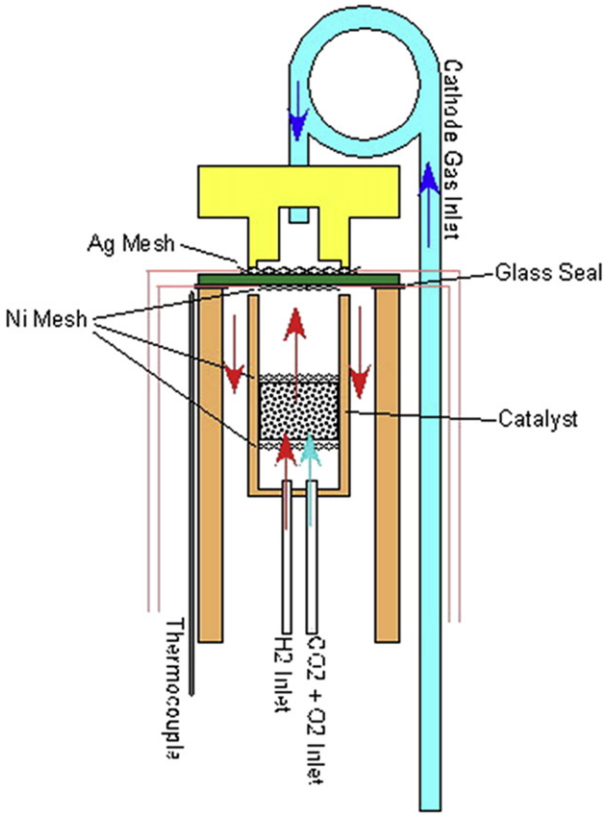

Fig. 2. Detail of cell mounting and catalyst placement.

2.2. Cell testing

Data was collected at 650, 700, 750 and 800 °C at pressures ranging from 101 kPa (1 atm) to 724 kPa (7.14 atm). The fuel was a synthetic reformate formulated to match the composition that would be obtained by steam reforming of kerosene with 85% anode recycle [21]. The mix was made by injecting 48.1% H_2, 44.4% CO_2 and 7.4% O_2 (200 cm^3 min^{-1} total) through the catalyst bed as shown in Fig. 2. The H_2 was introduced separately from the O_2 + CO_2. A nickel-based catalyst, Sud-Chemie G-90, was suspended between two layers of Ni mesh within an alumina cup held at the same temperature as the cell. The cup was positioned to leave a ~2 mm gap to the anode surface to serve as a gas outlet. 200 sccm of air was delivered to the cathode by means of a silver tube that ran up the length of the furnace alongside the alumina tube. Equilibrium was calculated for both the water–gas shift and the methanation reactions. The calculated equilibrium compositions ranged from 22% H_2, 13% CO, 29% H_2O, 35% CO_2, 0.2% CH_4 at 650 °C and 101 kPa to 17% H_2, 9% CO, 33% H_2O, 38% CO_2, 3.0% CH_4 at 650 °C and 724 kPa.

To activate the cell, it was held at 800 °C and 101 kPa at a constant voltage of 0.8 V until the current reached a constant value. Testing began by measuring the I–V curve from OCV to 0.75 V, as it was assumed that lower voltages are to be avoided because they have been shown to cause degradation [22]. The complex electrochemical impedance spectra were obtained at OCV, 0.9 V and 0.8 V using a Solartron 1470E/1255B multistat test system.

The pressure within the vessel was controlled by two backpressure regulators with one controlling the fuel side and the other controlling the air side. These backpressure regulators use a diaphragm and a controlling gas pressure to set their backpressure value. A common controlling gas was used to control both regulators and the backpressure difference between the air and fuel sides was less than 5 kPa. As the control pressure was ramped up, the backpressure regulators blocked the exhaust flow until the fuel and air side pressures reached the same level as the reference pressure, at which point normal exhaust flow resumed. The cell was held at OCV during such pressure changes. An I–V curve and impedance data were recorded at each pressure level. Temperature was then changed to a new level and the tests were repeated.

3. Results

The I–V data (points) are plotted in Fig. 3, each plot representing a different temperature, from 650 to 800 °C. At the higher pressures the mass flow controllers on the anode feed were somewhat erratic, causing some noise in the I–V data. Note that the horizontal scales in Fig. 3 are different to accommodate the higher currents at higher temperatures. The lines are fitted quadratics of the form,

$$V = Ai^2 + Bi + C \quad (5)$$

where V is the voltage, i is the current density (A cm^{-2}) and A, B, and C are the fitted coefficients. The coefficients and R-squared values are listed in Table 1. A is a measure of the I–V curvature, B is a measure of the slope and C is the experimentally measured OCV.

Increasing temperature by 150 °C increased power density by twice as much as did increasing pressure by a factor of seven, from 101 to 724 kPa. Fig. 4 is a plot of the I–V curves for increasing temperature, all at 101 kPa. The power density at 0.8 V increased from 0.100 at 650 °C to 0.400 W cm^{-2} at 800 °C, a factor of four. On the other hand, in Fig. 3d, as the pressure was increased from 101 to 724 kPa, at constant 800 °C, the power density at 0.8 V increased by a factor of 1.91. Comparing Fig. 3a–d, it is apparent that the upward curvature and the negative slope both decreased with increasing temperature and pressure. The boost due to a pressure increase became larger as temperature increased; there was an apparent positive interaction between the variables, pressure and temperature.

There are theoretical reasons to expect power density to increase logarithmically with pressure [18]. Fig. 5 is a plot of normalized power density at 0.8 V as a function of the natural logarithm of pressure. The magnitude of the effect of pressure on power density apparently increases with temperature, as discussed above. The data deviate from the fitted lines, having upward curvature, but becoming more linear as temperature increases. Fig. 6 is a plot of normalized power density at 0.2 A cm^{-2} as a function of the natural logarithm of pressure. Viewed this way, temperature apparently does not change the magnitude of the effect of pressure on power density, as the data for different temperatures are essentially superimposed. Fig. 7 is a plot of normalized power density as a function of the natural logarithm of pressure for a range of current densities, all taken at 800 °C. The magnitude of the effect of pressure on power density at constant current apparently increases with current density.

The cell resistance at each temperature was determined using electrochemical impedance spectroscopy. Typical complex impedance spectra obtained at 800 °C are shown in Fig. 8. Two separable arcs were clearly observed in all of the spectra, but the suppressed shape of each arc suggested that at least two equivalent circuits were needed to fit each arc. The following equivalent circuit was used to fit the impedance spectra: $LR_0(RQ)_1(RC)_2(RC)_3(RQ)_4$, where L is an inductance in series with R_0, an ohmic resistance, (RQ) is a circuit consisting of a resistance and a constant phase element, (RC) is a circuit consisting of a resistance and a capacitance. The annotations 1, 2, 3, and 4 indicate a time constant increase. The

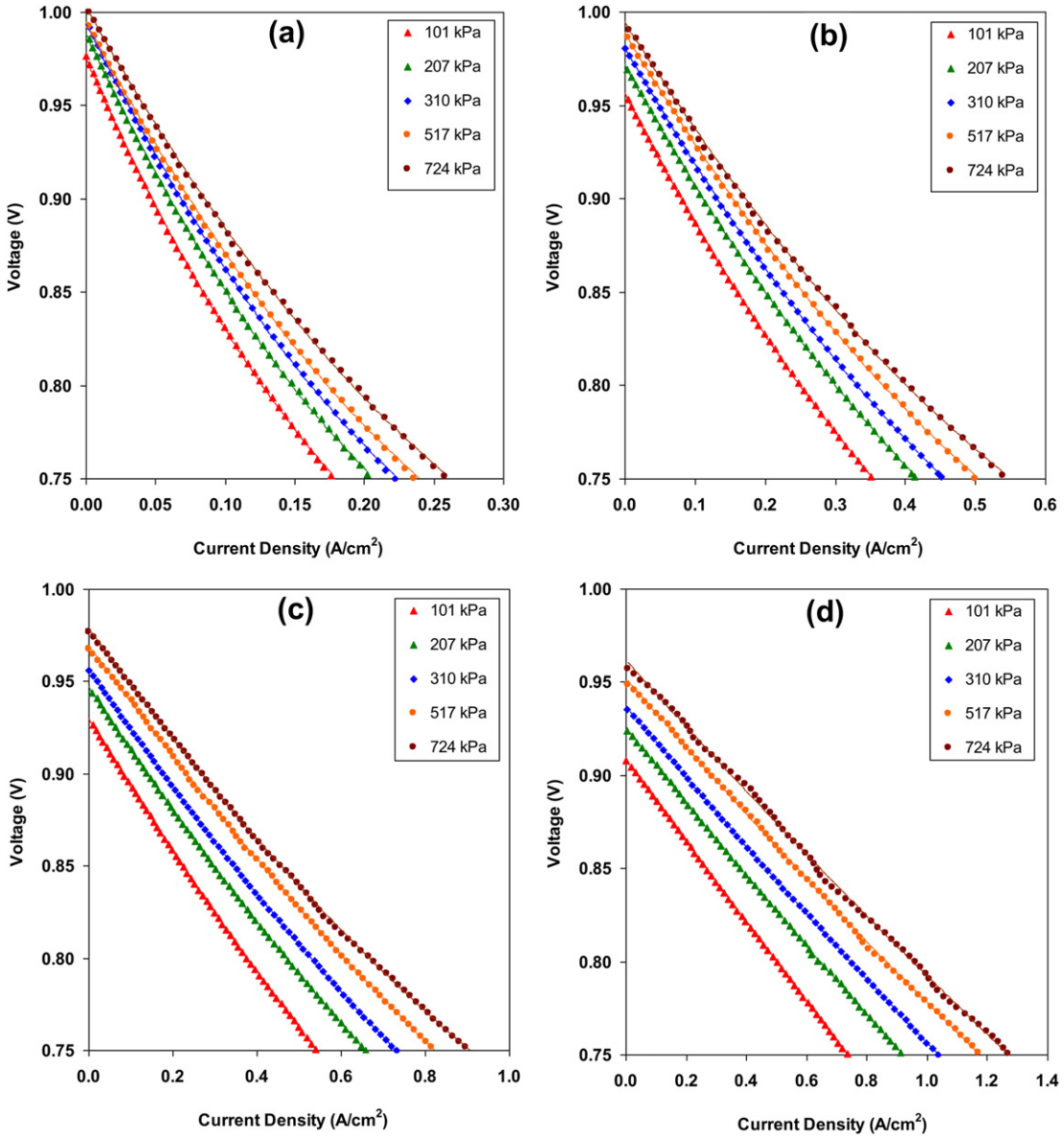

Fig. 3. I–V data (points) taken at pressures ranging from 101 to 724 kPa for a button cell with reformate on anode and air on cathode, (a) 650 °C, (b) 700 °C, (c) 750 °C, (d) 800 °C. The lines are fitted quadratics, whose coefficients are listed in Table 1.

ohmic and electrodic ($R_1 + R_2 + R_3 + R_4$) resistances at each pressure for different temperatures are given in Fig. 9. The activation energy for ohmic losses was 0.90 ± 0.02 eV. With the pressure increase to 724 kPa the ohmic losses at a given temperature remained nearly constant. The electrodic resistance dominated the total cell losses at all pressures and temperatures and was 2–4 times higher than the ohmic resistance (Figs. 8 and 9). It changed considerably with pressure. The pressure dependence at 650 °C had a slope of −0.18 ± 0.05, and the slope became steeper at higher temperatures (Fig. 10). Furthermore, the slope was generally steeper for a loaded cell, when it was held at 0.9 or 0.8 V, compared to that at open-circuit conditions. Slopes obtained at OCV and 0.8 V are included in the inset in Fig. 10. In general, the cell resistance obtained at 0.9 and 0.8 V was lower than that obtained at OCV (Fig. 11). When operated at lower temperatures, 650 and 700 °C, cell polarization had a larger effect on the cell resistance than the pressure increase: the cell resistance determined at 0.8 V and 0.9 V at 101 kPa was 20% lower than that at OCV at 724 kPa. At 750 °C the resistance decrease on polarization at 101 kPa was comparable to that at 724 kPa at OCV. At 800 °C the effect of pressure on the electrodic resistance prevailed.

From the Arrhenius plots of the electrodic resistance, an apparent activation energy of 1.28 ± 0.06 eV was calculated in the pressure range from 101 kPa to 724 kPa. For the cell tested at 0.8 V, the activation energy of the electrodic resistance was 0.96 ± 0.09 eV in the same pressure range.

For simplicity, each arc in the impedance spectrum in this paper is discussed as a sum of processes occurring at either high frequency (HF), or low frequency (LF) in the descending order of their relaxation frequency. The LF and HF features were separated from each equivalent circuit and plotted as a function of pressure. The trends observed at 800 °C at open-circuit conditions and at 0.8 and 0.9 V are given in Fig. 12. The largest contribution to the cell resistance came from the LF feature and those processes were dominant at all temperatures and voltages. The LF processes exhibited the strongest pressure dependence and decreased with increasing pressure as $P^{-0.32}$ to $P^{-0.38}$. The LF processes were not affected by cell voltage. The contribution of the HF feature to the

Table 1
Coefficients and *R*-squared values of quadratics fitted to the I–V curves in Fig. 3.

T (°C)	*P* (kPa)	*A*	*B*	*C*	R^2
650	101	2.511	−1.700	0.975	0.9998
650	207	2.116	−1.583	0.988	0.9998
650	310	1.818	−1.491	0.993	0.9998
650	517	1.539	−1.387	0.994	0.9998
650	724	1.347	−1.314	1.002	0.9997
700	101	0.426	−0.731	0.956	0.9997
700	207	0.354	−0.676	0.971	0.9999
700	310	0.323	−0.652	0.980	0.9999
700	517	0.290	−0.618	0.988	1.0000
700	724	0.274	−0.593	0.994	1.0000
750	101	0.083	−0.376	0.930	0.9999
750	207	0.075	−0.349	0.947	0.9999
750	310	0.068	−0.332	0.957	1.0000
750	517	0.054	−0.312	0.970	1.0000
750	724	0.065	−0.311	0.979	1.0000
800	101	0.009	−0.222	0.908	0.9993
800	207	0.014	−0.204	0.925	0.9997
800	310	0.012	−0.193	0.937	1.0000
800	517	0.014	−0.188	0.952	0.9999
800	724	0.010	−0.180	0.962	1.0000

cell resistance was smaller than that of LF at all temperatures. It was strongly influenced by the cell voltage and rapidly decreased when the cell was polarized. The pressure dependence was weaker compared to that of the LF processes, $P^{-0.11}$ at OCV and $P^{-0.21}$ at 0.8 V (Fig. 12).

4. Discussion

4.1. Effect of temperature and pressure on OCV

The measured OCVs were increasingly lower than the predicted values as temperature was increased. The measured OCVs are compared to the calculated OCVs in Fig. 13. The reason for this is unknown, however the largest discrepancy between measured and calculated OCVs (800 °C, 207 kPa) is only 0.0088 V. It should be obvious that OCVs should follow the Nernst equation, but they seldom do, presumably as a result of leaks in the test system or lack

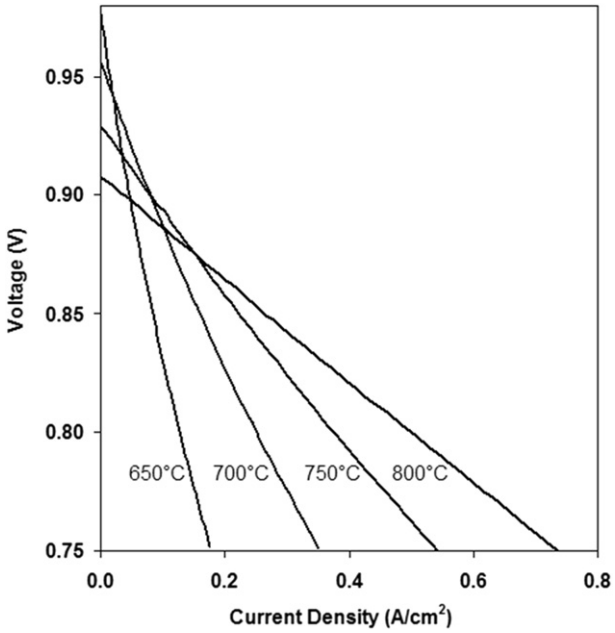

Fig. 4. Comparison of I–V curves from Fig. 3, all at 101 kPa, showing the effect of increasing temperature.

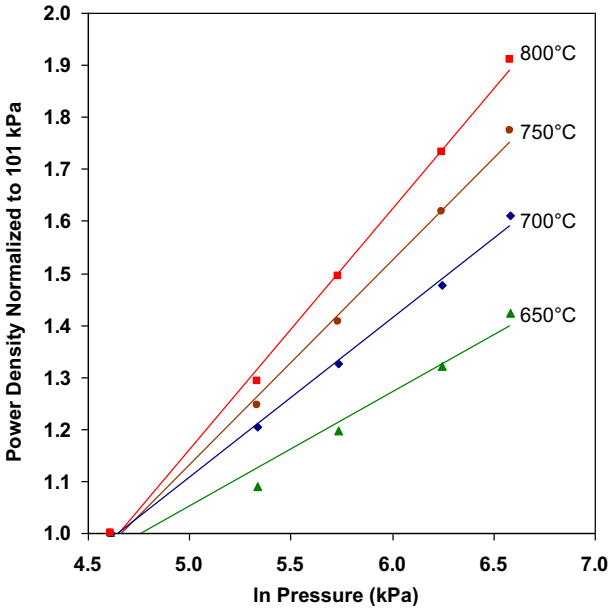

Fig. 5. Power density at 0.8 V normalized to 101 kPa plotted as a function of the natural logarithm of pressure. The lines were fitted by least squares.

of control over the anode gas composition [8,12,15]. To calculate the OCVs, we assumed the reformate was in equilibrium both relative to the water–gas shift reaction,

$$CO + H_2O \leftrightarrow CO_2 + H_2 \quad (6)$$

and to the methanation reaction,

$$3H_2 + CO \leftrightarrow CH_4 + H_2O \quad (7)$$

Because of the change in the number of moles of gas, methane formation increases at higher pressures. On the other hand, increasing temperature decreases methane formation. Calculated equilibrium methane content at 650 °C ranged from 0.2% at 101 kPa

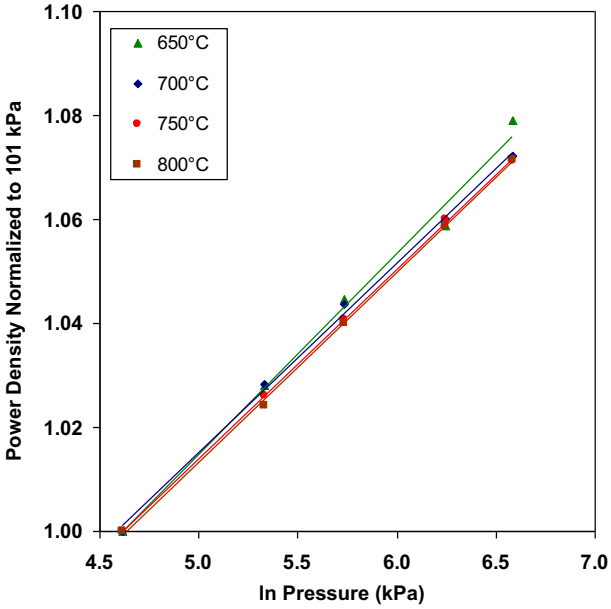

Fig. 6. Power density at 0.2 A cm^{-2} normalized to 101 kPa plotted as a function of the natural logarithm of pressure. The lines were fitted by least squares.

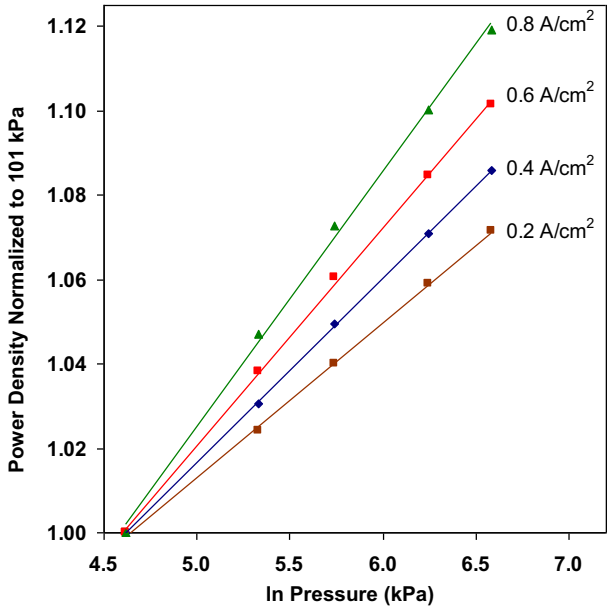

Fig. 7. Power density at constant current density for four current densities normalized to 101 kPa plotted as a function of the natural logarithm of pressure. All data were taken at 800 °C. The lines were fitted by least squares.

to 3% at 724 kPa. At 800 °C, methane content ranged from $\sim 2 \times 10^{-3}$% at 101 kPa to only 0.1% at 724 kPa. These effects combined to depress the OCVs at high pressure and low temperature (upper-right in Fig. 13) as more methane formed and hydrogen was removed from the equilibrated reformate while water was added. If methanation did not occur as pressure was increased from 101 kPa at 650 °C, the OCVs would have followed the broken line in Fig. 13. This effect of methanation explains the apparent positive interaction of temperature with pressure on the power boost. At 800 °C, the OCV changed from 0.916 to 0.961 V, an increase of 45 mV going from 101 to 724 kPa. At 650 °C, due to the methane formation, the similar increase is only 23 mV.

In contrast, the interaction between temperature and pressure should be much smaller for fuels that do not contain carbon, such as $H_2/N_2/H_2O$ mixtures. For 48.5% H_2, 3% H_2O balance N_2, the increase in OCV at 800 °C is 45 mV, while the increase at 650 °C is 39 mV.

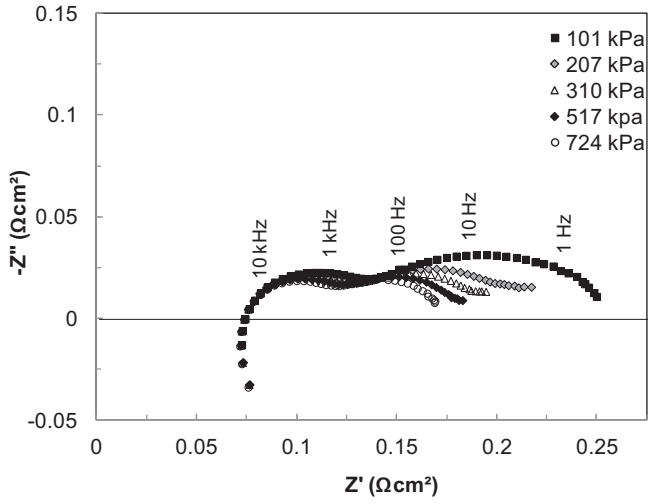

Fig. 8. Complex impedance spectra obtained at 800 °C at OCV at several different pressures.

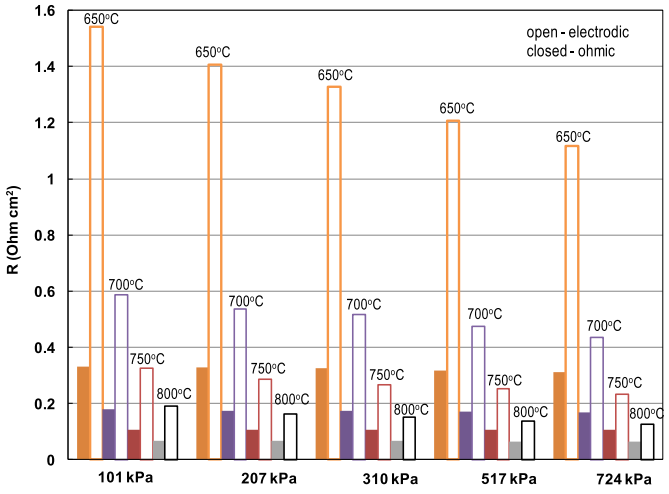

Fig. 9. Electrodic and ohmic resistances of the anode supported cell obtained at the OCV at different pressures.

4.2. Effect of pressure on kinetics versus OCV

In order to assess the effect of pressure on kinetics, the I–V curves taken at 750 °C, 101 and 724 kPa in Fig. 3c were fitted with quadratics of the form shown in Eq. 5. Fig. 14 shows those two I–V curves with the fitted quadratics. Two additional lines and their associated quadratics are shown in Fig. 14. Line K in Fig. 14 is a quadratic with the curvature and slope of the 724 kPa I–V curve, but with the OCV of the 101 kPa curve. Line K therefore represents the effect of boosting the kinetics alone. Line Q has the same curvature and slope as the 101 kPa I–V curve, but has the higher OCV of the 724 kPa I–V curve. Line Q therefore represents the effect of boosting the OCV alone. At 0.8 V the boost due to kinetics alone is 6.8% whereas the boost due to OCV alone is 13.0%, almost twice as large. This finding differs substantially from the statement in Henke et al. [17] that the effect of increasing OCV is rather small compared to the effects on kinetics.

Our impedance results also suggest that electrodic losses can be substantially lowered by operation of SOFCs at elevated pressures.

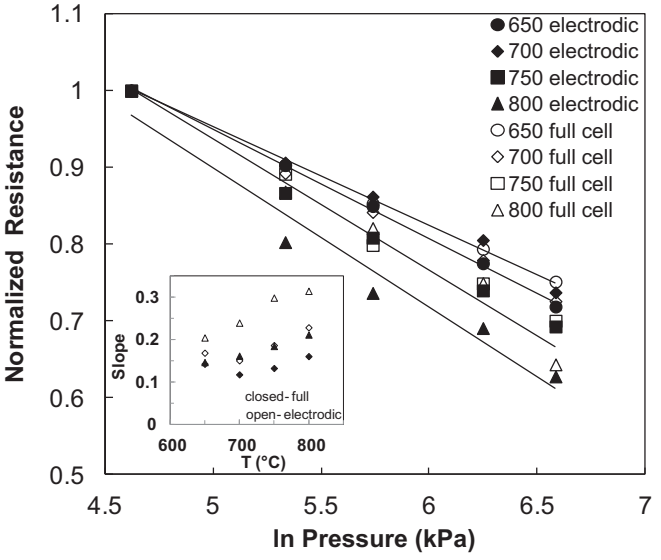

Fig. 10. Full cell resistances and electrodic resistances normalized to those at 101 kPa. Inset gives the slope values at each temperature at OCV (diamonds) and 0.8 V (triangles).

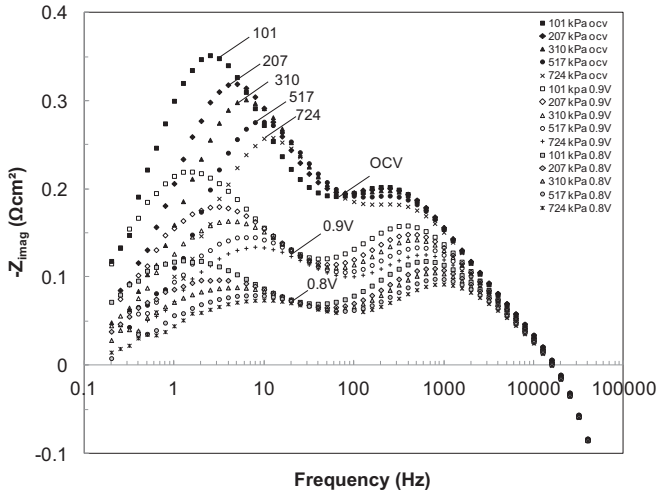

Fig. 11. Bode plot of impedance spectra obtained at 650 °C at OCV, 0.9 and 0.8 V at different pressures.

Two main features appearing in the impedance spectra decreased with the pressure increase to 724 kPa, but the dependence on pressure for each was different. The LF feature decreased proportionally to $P_{total}^{0.3-0.4}$ and the HF feature had a $P_{total}^{0.1-0.2}$ dependence. Each feature is likely to represent a combination of anodic and cathodic processes. In this study, no attempt was made to separate the anode and cathode contributions from the total electrodic losses. Yet, the HF features are often attributed in the literature to charge transfer reactions, while the LF features are attributed to processes such as adsorption, dissociation and diffusion [20]. The HF feature showed an approximately $P_{total}^{1/6}$ dependence, which would be reasonable to attribute to charge transfer reactions at the triple-phase boundary. This is also in agreement with the strong dependence on cell voltage. The LF feature showed a stronger pressure dependence of $P_{total}^{0.3-0.4}$ and very weak, if any, voltage dependence and could be attributed to any reaction involving adsorption, dissociation, or diffusion. The $P_{total}^{0.3-0.4}$ dependence is possibly a combination of ½ and ¼ dependences, which in principle are expected for a mixed conductor, such as LSCF. Similar 0.3–0.4 dependence was observed for the $(La_{0.8}Sr_{0.2})_{0.98}MnO_3$–ceria composite cathode [20] and was attributed to dissociative oxygen adsorption, while an $(La_{0.8}Sr_{0.2})_{0.98}MnO_3$ cathode that is primarily an electronic conductor exhibited a ¼ dependence on pressure.

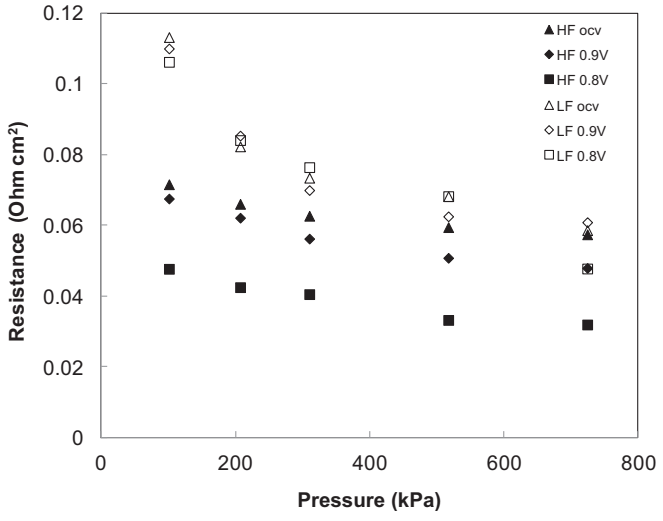

Fig. 12. Sum of resistances quantified in the high frequency (HF) and low frequency (LF) ranges by fitting the impedance spectra obtained at 800 °C at OCV, 0.9, and 0.8 V.

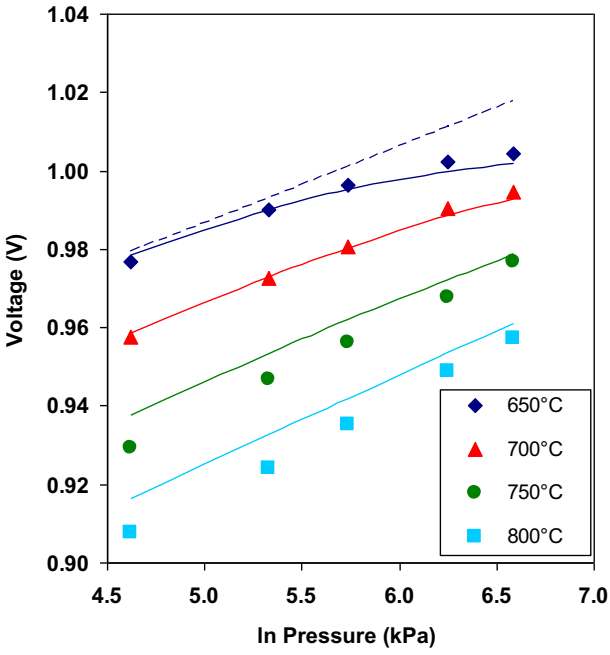

Fig. 13. Measured OCVs (points) compared to OCVs calculated for equilibrated reformate of steam reformed kerosene with 85% anode recycle (solid lines). The broken line shows how the OCV would change with increasing pressure at 650 °C if methanation *did not* occur.

4.3. Comparisons to literature

In order to compare our results to those of Henke et al. [17] and Jensen et al. [15], their I–V curves were carefully digitized and

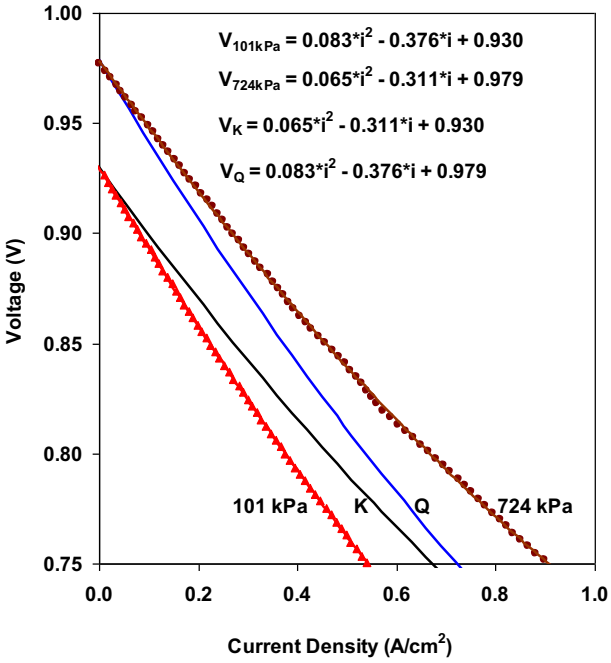

Fig. 14. I–V curves taken at 101 and 724 kPa at 750 °C. Line K illustrates the magnitude of effect of pressure on kinetics alone. Line Q illustrates the magnitude of effect of pressure on OCV alone.

interpolated by fitting quadratics. The data reported by Henke et al. [17] were taken on a 5-cell flow-through stack that is described in Seidler et al. [16]. The cells were Ni-YSZ anode supported with 10 μm YSZ electrolyte, 10 μm LSM–YSZ active cathode and 60 μm LSM current collector. Active area was 84 cm^2 per cell. Fig. 15 is a plot of normalized power density at 0.8 V as a function of natural logarithm of pressure, comparing the PNNL data at 800 °C to that of Henke et al. [17]. For the purpose of normalization, quadratics were fitted to the Henke data in order to estimate the power density they would have measured at 101 kPa. The PNNL data best match Henke's data taken at 50% fuel utilization. Note that Henke's data, like ours, deviate slightly from linearity, showing upward curvature, especially at the lower fuel utilizations.

The cell tested by Jensen et al. [15] was in planar configuration and had flow-through channels (cross-flow), unlike PNNL's button cell. The 16 cm^2 active area cell had a Ni-YSZ anode supporting a 10 μm YSZ electrolyte and a 20 μm LSM–YSZ cathode. The fuel used by Jensen et al., was a factor of about two more concentrated compared to PNNL's. Also, pure oxygen, rather than air, was fed to the cathode. Fig. 16 is a plot of normalized power density at 0.2 A cm^{-2} as a function of natural logarithm of pressure, comparing the PNNL data at 750 °C to that of Jensen et al. [15]. Jensen's original data deviate from the PNNL results at the highest pressure. However, this deviation is due to inconsistent OCVs. While Jensen's anode fuel was reported as 80% H_2 and 20% H_2O, all measured OCVs were 12–23 mV lower than expected for that fuel. At 101 kPa and 750 °C, their measured OCV, 1.039 V, indicates a composition of 74.5% H_2, balance steam. We used the fitted A and B coefficients for Jensen's I–V curves at higher pressures and substituted in *C* coefficients that were calculated based on the assumption of 74.5% H_2. The data taken from the corrected I–V curves lies almost exactly over the PNNL data in Fig. 16.

It is, perhaps, not surprising that our data, taken with an LSCF cathode is so similar to the Jensen et al. and Henke et al. data, which were taken with LSM–YSZ cathodes, because both LSCF and LSM–YSZ are mixed conductors.

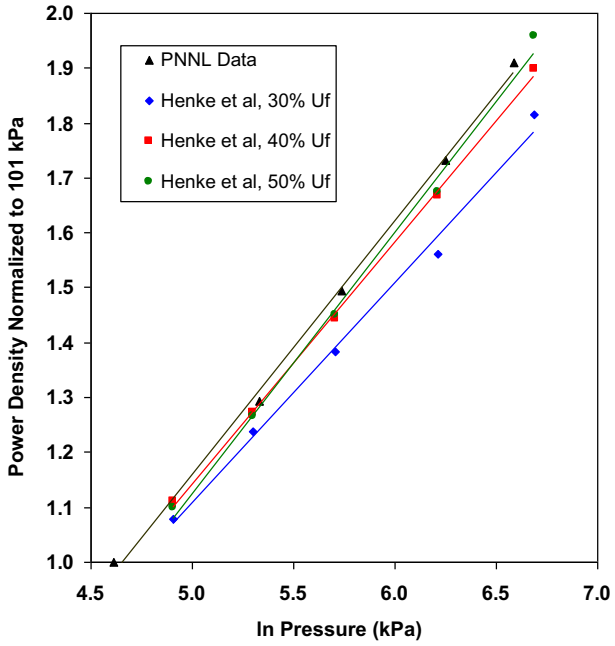

Fig. 15. Power density at 0.8 V normalized to 101 kPa plotted as a function of the natural logarithm of pressure. All data were taken at 800 °C. The data from Henke et al. [18] were taken by digitizing their I–V curves. The lines were fitted by least squares.

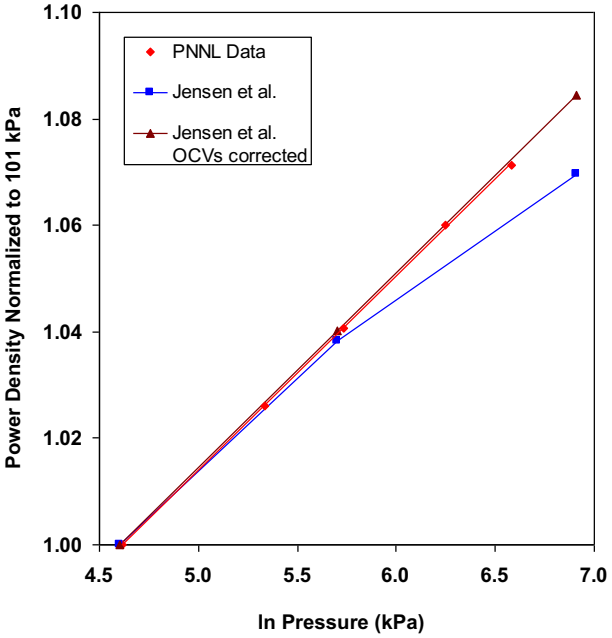

Fig. 16. Power density at 0.2 A cm^{-2} normalized to 101 kPa plotted as a function of the natural logarithm of pressure. All data were taken at 750 °C. The data from Jensen et al. [15] were taken by digitizing their I–V curves.

5. Conclusions

Using a Ni-YSZ anode-supported button cell with $La_{0.6}Sr_{0.4}Co_{0.2}Fe_{0.8}O_3$ (LSCF) cathode tested with air on the cathode and simulated steam reformate of kerosene on the anode, it was demonstrated that increasing the temperature from 650 to 800 °C increased the power density at 0.8 V by a factor of about four and increasing the pressure from 101 to 724 kPa increased the power density by a factor of about two. Power densities increased nearly linearly with the logarithm of pressure. Impedance spectroscopy results suggested that electrodic losses were substantially lowered at elevated pressures. An apparent positive interaction between the effects of temperature and pressure was mostly due to methanation increasing at lower temperatures and higher pressures. It was shown that the increase in power density due to the effect of pressure on the OCV was about twice as large as the increase due to the effect of pressure on kinetics. While our data were obtained from a cell with LSCF cathode, the performance boost due to pressure increase closely matched that for cells with LSM/YSZ cathodes.

Acknowledgments

This work was supported by the United States Department of Energy Office of Energy Efficiency and Renewable Energy. The authors appreciate helpful discussions with L.R. Pederson.

References

[1] S.C. Singhal, Solid State Ionics 135 (2000) 305–313.
[2] L. Magistri, A. Traverso, F. Cerutti, M. Bozzolo, P. Costamagna, A.F. Massardo, Fuel Cells 5 (2005) 80–96.
[3] W.J. Yang, S.K. Park, T.S. Kim, J.H. Kim, J.L. Sohn, S.T. Ro, J. Power Sources 160 (2006) 462–473.
[4] S.K. Park, T.S. Kim, J. Power Sources 163 (2006) 490–499.
[5] S.K. Park, K.S. Oh, T.S. Kim, J. Power Sources 170 (2007) 130–139.
[6] W. Burbank Jr., D. Witmer, F. Holcomb, J. Power Sources 193 (2009) 656–664.

[7] F. Leucht, W.G. Bessler, J. Kallo, K.A. Friedrich, H. Muller-Steinhagen, J. Power Sources 196 (2011) 1205–1215.
[8] S.C. Singhal, Recent Progress in Tubular Solid Oxide Fuel Cell Technology. Proceedings of the Fifth International Symposium on Solid Oxide Fuel Cells (SOFC – V), The Electrochemical Society, Inc, Pennington, NJ, 1997, pp. 37–50.
[9] N. Minh, Solid oxide fuel cell hybrid system for distributed power generation. Presented at the Second DOE/UN International Conference and Workshop on Hybrid Power Systems, April 16–17, 2002. http://www.netl.doe.gov/publications/proceedings/02/Hybrid/hybrid02.html.
[10] Fuel Cell Handbook, sixth ed., 2002, DOE/NETL-2002/1179.
[11] T.H. Lim, R.H. Song, D.R. Shin, J.I. Yang, H. Jung, I.C. Vinke, S.S. Yang, Int. J. Hydrogen Energy 33 (2008) 1076–1083.
[12] L. Zhou, M. Cheng, B. Yi, Y. Dong, Y. Cong, W. Yang, Electrochim. Acta 53 (2008) 5195–5198.
[13] S. Hashimoto, H. Nishino, Y. Liu, K. Asano, M. Mori, Y. Funahashi, Y. Fujishiro, J. Fuel Cell. Sci. Technol. 5 (2008) 031208-1–031208-5.
[14] S. Hashimoto, H. Nishino, Y. Liu, K. Asano, M. Mori, Y. Funahashi, Y. Fujishiro, J. Electrochem. Soc. 155 (2008) B587–B591.
[15] S.H. Jensen, X. Sun, S.D. Ebbesen, R. Knibbe, M. Mogensen, Int. J. Hydrogen Energy 35 (2010) 9544–9549.
[16] S. Seidler, M. Henke, J. Kallo, W.G. Bessler, U. Maier, K.A. Friedrich, J. Power Sources 196 (2011) 7195–7202.
[17] M. Henke, C. Willich, C. Westner, F. Leucht, R. Leibinger, J. Kallo, K.A. Friedrich, Electrochim. Acta 66 (2012) 158–163.
[18] M. Henke, J. Kallo, K.A. Friedrich, W.G. Bessler, Fuel Cells 11 (2011) 581–591.
[19] R.S. Gemmen, J. Trembly, J. Power Sources 161 (2006) 1084–1095.
[20] E.C. Thomsen, G.W. Coffey, L.R. Pederson, O.A. Marina, J. Power Sources 191 (2009) 217–224.
[21] M. Powell, K. Meinhardt, V. Sprenkle, L. Chick, G. McVay, J. Power Sources 205 (2012) 377–384.
[22] S. Koch, P.V. Hendriksen, M. Mogensen, Y.L. Liu, N. Dekker, B. Rietveld, B. de Haart, F. Tietz, Fuel Cells 6 (2006) 130–136.